Resonant mode interactions in Rayleigh-Bénard convection

Joana Prat,[1] Isabel Mercader,[2] and Edgar Knobloch[3]
[1]*Departament de Matemàtica Aplicada i Telemàtica, Universitat Politècnica de Catalunya, Barcelona, Spain*
[2]*Departament de Física Aplicada, Universitat Politècnica de Catalunya, Barcelona, Spain*
[3]*Department of Physics, University of California, Berkeley, California 94720*
(Received 5 February 1998)

In systems with midplane reflection symmetry the dominant spatial resonance is the 1:3 resonance. Numerical continuation is used to study this and other $1:2k+1$ resonances in two-dimensional convection between no-slip perfectly conducting horizontal plates. Periodic boundary conditions are imposed in the horizontal. These resonances influence the process of wave number selection at moderate Rayleigh numbers through the generation of hybrid solutions, and thereby modify the Eckhaus picture of wave number selection. Unlike the better known mixed modes the hybrid solutions have the same symmetry as a pair of primary rolls. Both hybrid and symmetry-breaking mixed modes are computed and their linear stability properties with respect to perturbations preserving different spatial periods are determined. A complete description of the effects of midplane reflection on wave number selection emerges. Only steady solutions are considered and the Prandtl number is fixed at $\sigma=10$. [S1063-651X(98)05709-2]

PACS number(s): 47.20.Ky, 05.45.+b

I. INTRODUCTION

The generation of mean flows by Reynolds stresses is a problem of fundamental importance in fluid dynamics. Although of primary importance in the theory of turbulence and turbulent convection, closely related issues arise in connection with ordered structures such as are present in convection at moderate Rayleigh numbers. Many studies of convection employ the analytically convenient stress-free boundary conditions at top and bottom. The resulting system is then invariant under Galilean boosts, i.e., the boundaries do not select a preferred rest frame. As a result convection rolls are neutrally stable with respect to such boosts, and the solutions are only defined up to an arbitrary constant horizontal velocity. For spatially periodic patterns this arbitrariness is of no consequence. However, spatially inhomogeneous patterns can drive horizontal mean flows, and do so arbitrarily close to onset of the primary convective instability. With no-slip boundary conditions at top and bottom the system is no longer Galilean invariant and the excitation of mean flows becomes harder. Such flows are now the result of secondary symmetry-breaking instabilities [1]. Typically these arise as a result of a coherent tilt of the convection cells; such a tilt generates a nonzero Reynolds stress, which in turn drives the associated mean flow. This mechanism is well known and has been explored in several different contexts [2,3]. It is particularly important when the cells are *narrow* [4,5]. In the studies mentioned above the cell width is imposed arbitrarily and is smaller than that predicted on the basis of linear stability theory of the conduction state. The question therefore arises whether there are mechanisms responsible for generating mean flows that operate for cells of the naturally preferred scales. To this end we investigate secondary branches arising from the interaction of two distinct *horizontal* modes. We find that, depending on their symmetries, some of these are accompanied by large-scale mean flows, while others are not. This mechanism for mean flow generation is distinct from the coherent tilt alluded to above, which comes about from the excitation of the second *vertical* mode of the system.

With this motivation in mind we focus on two-dimensional Rayleigh-Bénard convection with periodic boundary conditions in the horizontal, choosing a large spatial period compared to the period of the primary roll pattern. Since we impose identical boundary conditions at the top and bottom, the resulting system has an additional midplane reflection symmetry. The usual perception is that this symmetry is irrelevant in two dimensions. We show here that in laterally unbounded systems this is not in fact so. This is because of the role played by spatial resonances. The requirement that the amplitude equations commute with the midplane reflection symmetry changes the structure of the 1:2 resonance and gives the 1:3 resonance unexpected prominence. This is so *despite* the fact that the 1:2 resonance occurs at lower Rayleigh numbers, and is a consequence of the fact in the 1:2 resonance the midplane reflection symmetry pushes the resonant terms to fifth order [6,7] thereby destroying much of the dramatic behavior present in the generic case [8]. In particular, pure modes with wave numbers $n=1,2$ now bifurcate from the conduction state. In contrast, the 1:3 resonance is unaffected by the midplane reflection and the resonant terms enter at third order. As a consequence the $n=1$ mode becomes a *hybrid* state and the effects of this resonance much more dramatic. This is because the $n=1$ and $n=3$ states have the same symmetry properties and so interact much more strongly than the corresponding $n=1$ and $n=2$ states in the 1:2 interaction. In this paper we examine the role played by the 1:3 resonance and show that it and other odd:odd resonances play a major role in stabilizing different types of solutions. For the study we employ symmetric no-slip boundary conditions at the top and bottom but do not impose any restrictions on the parity of the solutions in the vertical. We identify two types of steady solutions, those with the same symmetry as the primary rolls (hereafter referred to as *hybrid* solutions) and those that break this symmetry (hereafter referred to as *mixed* solutions). The former

 © 1998 The American Physical Society

involve a contribution from two odd modes which varies gradually with the bifurcation parameter, and may arise in a primary bifurcation. The latter are only produced in secondary bifurcations but may be accompanied by mean flows. Although none of the nonzero-mean-flow solutions are stable at the low to moderate Rayleigh numbers considered, we find that they play a critical role in the stabilization of various solution branches that are unstable near onset, and as a result obtain a fairly complete understanding of the multiplicity of coexisting solutions near onset. We do not consider here the large Rayleigh numbers studied by Prat *et al.* [5] at which oscillations set in.

The present paper sheds considerable light on the process of wave number selection far from onset. Close to onset this process is described by the Ginzburg-Landau equation. The resulting Eckhaus picture of wave number selection is based on the sideband instability of plane wave solutions of this equation within their domain of existence. The Busse ''balloon'' summarizes the extension of calculations of this type to larger amplitude rolls and hence to larger values of the Rayleigh number Ra. However, all such calculations are based on the stability properties of a single roll state with wave number near the critical wave number k_c. Consequently spatial resonances are absent from the analysis. Moreover, the possibility that the roll state becomes unstable to instabilities generating mean flows is also not considered. In this paper we find that both of these complications become important as the Rayleigh number is increased, and that both modify the stability properties of the basic roll state in new ways. The paper can be thought of as a generalization of the work of Mizushima and Fujimura [9] (hereafter referred to as MF) on the 1:3 resonance with no-slip boundary conditions. These authors were the first to observe, using a coupled amplitude equation description, that the resonance modified the type and multiplicity of solutions present above threshold, and concluded that the Eckhaus picture of wave number selection was oversimplified. However, the MF approach suffers from the limited validity of the amplitude equations employed. In addition these equations were constructed only for modes of like parity in the vertical. In the present paper we avoid both limitations by eschewing the amplitude equation approach entirely and resorting to numerical continuation techniques to follow solution branches from threshold towards higher Rayleigh numbers. These techniques enable us to trace the stability changes either with increasing Ra or with increasing spatial period and to identify the secondary states produced in the resulting bifurcations. We compute such secondary states and classify them according to their symmetry properties and associated mean flows. The outcome is a fully nonlinear picture of wave number selection in systems with midplane reflection symmetry. This picture resembles that put forward for the Eckhaus instability in Ref. [10] but includes additional destabilizing mechanisms absent from the Ginzburg-Landau description.

The paper is organized as follows. In Sec. II we derive the equations and describe the method used to determine both the primary roll states in the fully nonlinear regime and their stability properties. The results for Prandtl number $\sigma=10$ are presented in Sec. III. In Sec. IV we provide a theoretical explanation of some of our results. The paper concludes with a discussion in Sec. V. The essential group-theoretic considerations are summarized in two Appendixes.

II. THE EQUATIONS AND THEIR ANALYSIS

We consider two-dimensional Boussinesq thermal convection in a periodic horizontal layer and include the possibility of generating a nontrivial mean flow. Consequently, we split the solenoidal velocity field $\mathbf{v}(x,z,t)$ into its mean and fluctuating components,

$$\mathbf{v}=\mathbf{U}(z,t)+\mathbf{v}'(x,z,t),$$

where $\mathbf{U}=(U,0)$, $\mathbf{v}'=(-\partial_z\chi',\partial_x\chi')$ and $\bar{\mathbf{v}}'=\overline{\chi'}=0$, with the overline indicating an average over the horizontal period. The temperature $T(x,z,t)$ is written as

$$T=\tfrac{1}{2}-z+\theta(x,z,t).$$

Equations for U, χ', and θ are obtained from the horizontal average of the Navier-Stokes equations, the deviation of the vorticity equation from its horizontal average, and the heat equation. In nondimensional form, we obtain

$$(\partial_t-\sigma\partial_{zz}^2)U+\partial_z\overline{v_x'v_z'}=0, \tag{1a}$$

$$(\partial_t+U\partial_x-\sigma\nabla^2)\omega'+\mathrm{Ra}\ \sigma\partial_x\theta+\partial_{zz}^2U\partial_x\chi' +\frac{\partial(\chi',\omega')}{\partial(x,z)}-\overline{\frac{\partial(\chi',\omega')}{\partial(x,z)}}=0, \tag{1b}$$

$$(\partial_t+U\partial_x-\nabla^2)\theta-\partial_x\chi'+\frac{\partial(\chi',\theta)}{\partial(x,z)}=0, \tag{1c}$$

where $\omega'=-\nabla^2\chi'$, lengths and time have been expressed in units of the layer depth and thermal diffusion time in the vertical, respectively, and Ra and σ are the Rayleigh and Prandtl numbers. The boundary conditions are taken to be periodic in x with period L and no-slip, perfectly conducting in z:

$$U=\chi'=\partial_z\chi'=\theta=0 \quad \text{at} \quad z=\pm\tfrac{1}{2}. \tag{1d}$$

The equations are thus defined on the domain $(x,z)\in[0,L]\times[-\frac{1}{2},\frac{1}{2}]$. The resulting problem is solved numerically using a spectral Galerkin-Fourier technique in x and collocation Chebyshev in z [11].

Equations (1) are equivariant under the two reflections,

$$R_0:\quad (x,z)\to(-x,z),\quad (U,\chi',\theta)\to(-U,-\chi',\theta), \tag{2a}$$

$$\kappa:\quad (x,z)\to(x,-z),\quad (U,\chi',\theta)\to(U,-\chi',-\theta), \tag{2b}$$

and translations through a distance l,

$$T_l:\quad (x,z)\to(x+l,z),\quad (U,\chi',\theta)\to(U,\chi',\theta). \tag{2c}$$

The reflection (2a) is with respect to an arbitrarily chosen origin in x; reflections R_{l_0} with respect to a plane $x=l_0$, say, are obtained by conjugation: $R_{l_0}=T_{l_0}R_0T_{-l_0}$. These symmetries generate the symmetry group $\Gamma=O(2)\times Z_2$. The conduction state $U=\chi'=\theta=0$ is invariant under this group.

The primary instability of this state is to a nontrivial roll state $(0,\chi',\theta)$ that breaks the translation symmetry T_l but is invariant under a reflection R_{l_0} for an appropriate l_0 and the *shift-reflect* operation $T_{a/2}\kappa$, where $a \equiv L/n$ is the pattern wavelength (see Appendix A). Each of these symmetries is a generalized reflection in the sense that its square is the identity. It follows that the symmetry group of such a roll state is $G \equiv Z_2 \times Z_2 = D_2$, a subgroup of $O(2) \times Z_2$ [5]. In contrast an individual roll is invariant only under a 180° rotation. For a pattern with a node at $x=0$ this symmetry is $P = R_{a/4}\kappa$ and is sometimes referred to as a *point* symmetry. This symmetry acts on the fields as follows:

$$P: \quad (x,z) \to \left(\frac{a}{2} - x, -z\right), \quad (U,\chi',\theta) \to (-U,\chi',-\theta). \tag{2d}$$

Note that $P = R_0 T_{a/2}\kappa$ (since $T_{l_0} R_0 T_{l_0} = R_0$) and so $P \in G$. In the following we shall use the symbol R to refer to the reflection R_{l_0} for *suitable* l_0.

Note that the symmetry R of the primary flow implies that no mean flow is present: $U(z) \equiv 0$. This is not necessarily so for the states produced in secondary bifurcations from the primary rolls, as discussed below. These bifurcations typically break the symmetry G of the roll state and we summarize in Appendix A the various possible ways this can happen.

Numerically, the presence of D_2 symmetry implies that a roll state of wavelength a can be written in the form

$$\chi(x,z) = \sum_{k=1}^{K} \sum_{m=0}^{M} \chi_{km} f_m(2z) \sin(k\alpha x),$$

$$\theta(x,z) = \sum_{k=0}^{K} \sum_{m=0}^{M} T_{km} g_m(2z) \cos(k\alpha x),$$

relative to a suitable origin. Here $k+m$ is odd, $\alpha = 2\pi/a$ and the $f_m(2z)$, $g_m(2z)$ are suitable combinations of Chebyshev polynomials satisfying the boundary conditions. If the spatial period L is fixed at $L=a$ the above expansion describes a single pair of rolls bifurcating from the conduction state at a given critical Rayleigh number; this Rayleigh number is the same for two pairs of rolls bifurcating in a container of twice the length, $L=2a$, etc. As a consequence, one can obtain the neutral stability curve for n pairs of rolls from that for a single pair of rolls in a domain of width L simply by replacing L with nL (see Fig. 1). Thus $n = L/a$ measures the number of roll pairs in a given spatial period; it is also the wave number of the state. We say that a (spatial) resonance occurs when two different multiroll solutions bifurcate simultaneously from the conduction state. This situation corresponds to the intersection of different neutral stability curves in Fig. 1. In the following we refer to the intersection of two such curves with wave numbers n_1, n_2 as an $n_1{:}n_2$ resonance. Note that the first such intersections that are encountered always involve *adjacent* wave numbers ($|n_1 - n_2| = 1$). However, despite the fact that the $1{:}2k+1$, $k=1,2,\ldots$, resonances are shielded (see Fig. 1), they are responsible for a number of states found in the fully nonlinear regime, as described in Sec. III.

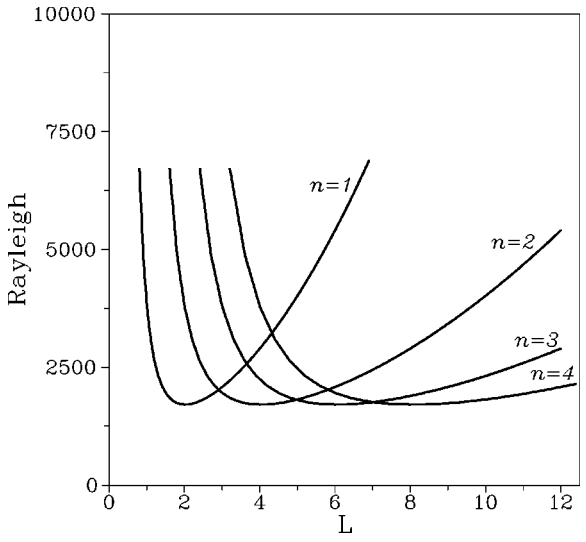

FIG. 1. Marginal stability curves for several multiroll solutions.

In order to study the stability of a multiroll solution, say a periodic solution with n pairs of rolls each of length a, we must consider all perturbations with period na. The basic solution has period a and hence the associated linear operator also has period a. From Floquet theory we know that the set of perturbations can be split up as [12]

$$\{w_m(x,z) e^{i d_m \alpha x} e^{\lambda_m t}\}_{m=0,\ldots,n-1}, \tag{3a}$$

where

$$w_m(x,z) = w_m(x+a,z), \tag{3b}$$

and $d_m = m/n \in [0,1)$.

The case $d_0 = 0$ corresponds to the study of the stability of a single pair of rolls (the $n=1$ case) since the perturbations all have the same period a as the rolls. In this case, as shown in [5], the perturbations split further into four invariant subgroups. Two of these generate solutions with nonzero mean flow $U(z)$, one with the symmetry P and the other with symmetry $T_{a/2}\kappa$ (see Appendix A). It follows from Eqs. (2) that in the former case the associated mean flow has an antisymmetric profile while in the latter the profile is symmetric. The remaining two perturbation types produce solutions that are invariant under R and G, respectively, and hence do not generate mean flows.

In the case $d \neq 0$ the basic period a is now broken and a new pattern with a larger period emerges. If the linear operator describing the stability problem is real, the eigenfunctions for the problem with d_m can be obtained by conjugating those with d_{n-m}; moreover $\lambda_m = \overline{\lambda}_{n-m}$. In this case it suffices to consider perturbations with $d_m \in (0,1/2]$,

$$d_m = 1/n, \ldots, 1/2.$$

In the present problem, the invariance of the primary roll solution under the reflection symmetry R imposes the stronger requirement $\lambda_m = \lambda_{n-m}$, with the corresponding eigenfunctions related by R.

These instabilities produce secondary branches of solutions with smaller symmetry. Since these solutions may be associated with mean flows we now write

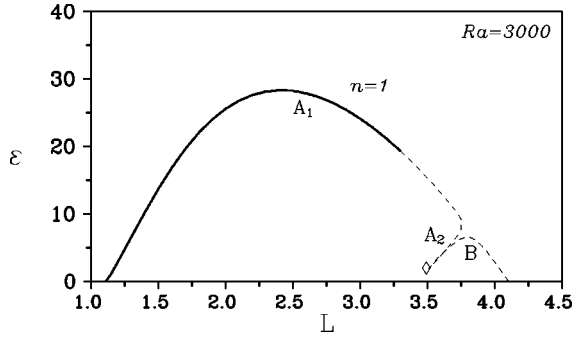

FIG. 2. Amplitude $\epsilon \equiv (1/2)v_x^2(L/4,1/4)$ of steady $n=1$ solutions as a function of the spatial period L for $\sigma=10$, Ra$=3000$. Solid (broken) lines denote stable (unstable) solutions. Only G-symmetric solutions are shown.

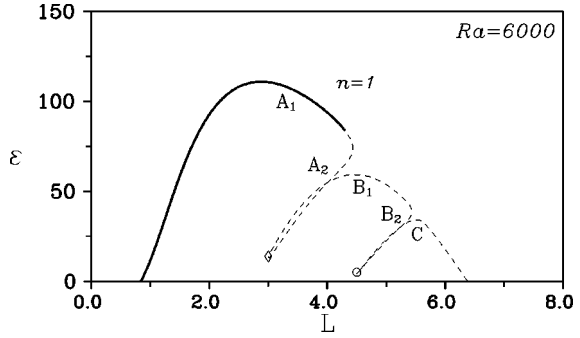

FIG. 3. Amplitude $\epsilon \equiv (1/2)v_x^2(L/4,1/4)$ of steady $n=1$ solutions as a function of the spatial period L for $\sigma=10$, Ra$=6000$. Solid (broken) lines denote stable (unstable) solutions. Only G-symmetric solutions are shown.

$$U(z)=\sum_{m=0}^{M} U_m g_m(2z),$$

$$\chi(x,z)=\sum_{k=-K}^{K}\sum_{m=0}^{M} \chi_{km} f_m(2z) e^{ik\alpha x},$$

$$\theta(x,z)=\sum_{k=-K}^{K}\sum_{m=0}^{M} T_{km} g_m(2z) e^{ik\alpha x},$$

where now $\alpha=2\pi/L$. The stability of these solutions is calculated as for the D_2-symmetric rolls except that now the perturbations for the $d_0=0$ case no longer split into four subgroups.

Since all solutions of interest in this paper are steady we solve Eqs. (1) using a Newton-Raphson iterative scheme with $K\leqslant 12, M\leqslant 24$. This resolution suffices for the modest values of the Rayleigh number considered. The stability properties of the resulting solutions are determined by solving the linear stability problem for the perturbations (3).

III. RESULTS

This section is divided into two parts. In the first we show, for fixed Rayleigh number, the effect of the $1:2k+1$ resonances on the generation of steady solutions that have the same symmetries as the primary convection rolls. In the second part, we choose two values of the spatial period close to $L^*=3.647$ (for which the 1:3 resonance takes place), and consider the influence of *other* resonances as the Rayleigh number is increased. All results are obtained for Prandtl number $\sigma=10$.

A. Transitions at constant Rayleigh number

Primary roll solutions consisting of a single pair of rolls ($n=1$) have been calculated at Rayleigh number Ra$=3000$ and their stability analyzed. One expects that such solutions do not exist if the imposed spatial period L is either too small or too large, for a fixed value of Ra. This expectation is borne out in Fig. 2, which shows the amplitude of these solutions [as measured by $\epsilon \equiv \frac{1}{2}v_x^2(x=\frac{L}{4}, z=\frac{1}{4})$] as a function of the spatial period L; dashed lines represent unstable solutions and solid lines stable ones. However, the figure also reveals that the situation is more complex. The figure reveals the presence of two peaks, the higher peak consisting of *two* families of solutions denoted by A_1 and A_2 and separated by a turning point (saddle-node bifurcation). The lower peak corresponds to a family of solutions denoted by B; A_2 and B are always unstable. For some periods L all three $n=1$ solutions coexist. The A_2 and B branches bifurcate together from a branch of $n=3$ multiroll solution (not shown) as discussed further below.

For this value of the Rayleigh number our results agree with those obtained by MF. However, at larger Rayleigh numbers they begin to differ. For example, at Ra$=6000$, the bifurcation diagram for the $n=1$ steady solutions looks like *three* peaks (see Fig. 3). The highest peak corresponds to the family of solutions A_1 with A_2 again separated by a saddle-node bifurcation. The next peak corresponds to solutions labeled B_1 and B_2, while the smallest peak corresponds to a new family of solutions, labeled C. Solutions A_2, B, and C are always unstable; this time it is the branches A_2 and B_1 that meet on an $n=3$ branch, while B_2 and C meet on an $n=5$ branch, neither of which is shown. The nature of these bifurcations can be gleaned from the bifurcation diagrams shown in Fig. 4. Figure 4(a) shows the first Fourier coefficient $\chi_1(z=\frac{1}{4})$ for both $n=1$ and $n=3$ solutions as a function of the spatial period L near the bifurcation point, indicated by a diamond in Fig. 3. The figure reveals the presence of a transcritical bifurcation from the $n=3$ state that gives rise to the two families A_2 and B_1 of $n=1$ states. The $n=3$ state has two unstable eigenvalues, each of double multiplicity prior to the transcritical bifurcation ($L<2.965$). This is a consequence of the fact that the primary instability to the $n=3$ state is preceded by loss of stability to $n=2$ and $n=1$ states; the unstable eigenvalues of the conduction state are inherited by the $n=3$ branch. At the transcritical bifurcation ($L=2.965$) one of these pairs moves to the left half of the complex plane so that for $L>2.965$ the $n=3$ branch has only one unstable eigenvalue of double multiplicity. In contrast the A_2 and B_1 branches each have three unstable eigenvalues near the bifurcation, with B_1 acquiring a fourth unstable eigenvalue beyond the saddle-node bifurcation. Bifurcations of this type have been found in two-dimensional thermosolutal convection [13]. In contrast, the bifurcation that is responsible for the families B_2 and C of $n=1$ solutions that bifurcate from an $n=5$ state at the point marked

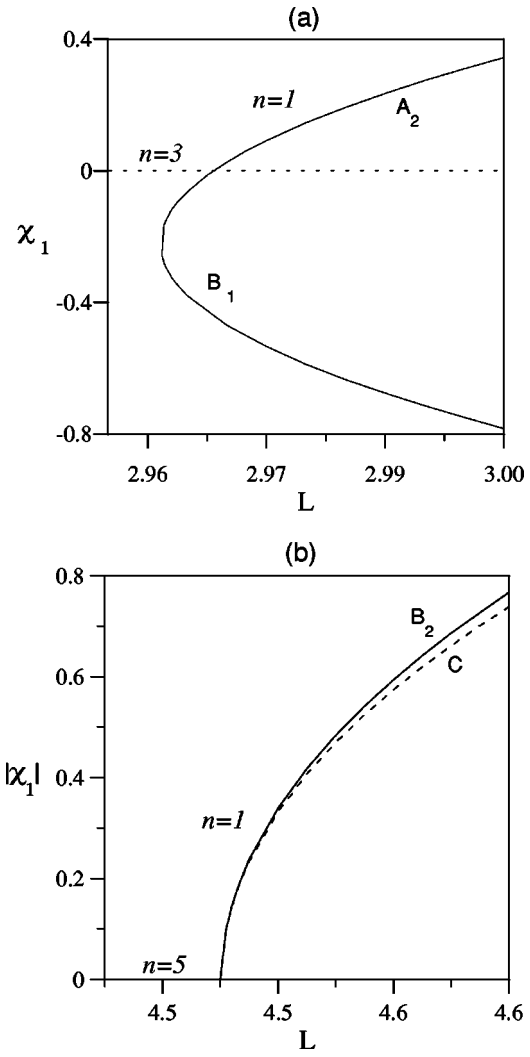

FIG. 4. (a) The transcritical bifurcation for Ra=6000 from $n=3$ multirolls to $n=1$ solutions, shown in terms of the first Fourier coefficient, $\chi_1(z=\frac{1}{4})$, as a function of L. (b) The bifurcation for Ra=6000 from $n=5$ multirolls to $n=1$ solutions, shown in terms of the modulus of the first Fourier coefficient, $|\chi_1(z=\frac{1}{4})|$, as a function of L. All solutions are unstable.

with a circle in Fig. 3 is quite different, and both B_2 and C bifurcate in the *same* direction [Fig. 4(b)]. Both bifurcations are discussed in Sec. IV.

In Fig. 5 we show, for Ra=6000, the streamlines corresponding to the different $n=1$ solutions that coexist at $L=3.8$, $L=5$, and $L=6$. All of these solutions share the symmetries of a single pair of rolls (i.e., the symmetry G) and all are unstable except for A_1 ($L=3.8$). The streamlines of the large amplitude states A_1, B_1, and $L=6$ look similar and have the structure formed in the primary instability. Indeed we can consider the envelope of the three peaks as a single family of solutions that has been interrupted by the 1:3 and 1:5 resonances. It is these resonances that are responsible for the hybrid structure of the states A_2, B_1, and B_2, C, respectively. This conclusion is supported by Fig. 6, which shows the critical Rayleigh number as a function of the spatial period L; the points where $n=3$ and $n=5$ multiroll solutions bifurcate from $n=1$ solutions are indicated by diamonds and open circles, respectively. The diamonds fall on a

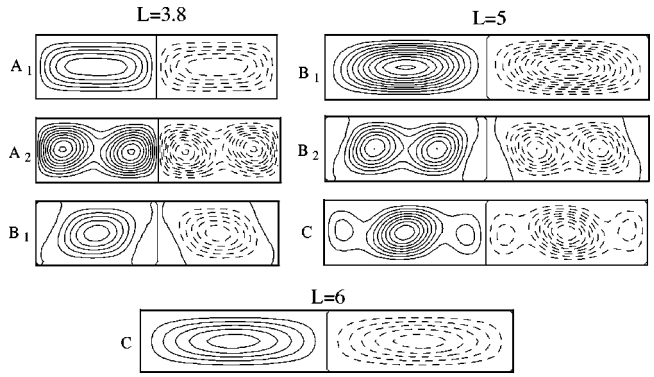

FIG. 5. Streamlines of the different steady $n=1$ solutions at $L=3.8$, $L=5$, and $L=6$ when $\sigma=10$, Ra=6000. All of these solutions are G symmetric.

curve that appears to emerge from the point $P_{1,3}$ where the 1:3 resonance is located, while the circles fall on a curve that appears to emerge from the location $P_{1,5}$ of the 1:5 resonance. Despite the differences between the different sets of streamlines in Fig. 5 *all* of the solutions shown are properly thought of as *hybrid* solutions. This is because in the presence of other modes ($n>1$) there is *no* pure $n=1$ mode (see Appendix B). In particular, while the A_1 state shown in Fig. 5 looks like a pure mode it does in fact contain a small contribution from the $n=3$ state; this is simply a consequence of the fact that this is a nonlinear state. This contribution gradually increases as one traverses the A_1 branch, and becomes visible to the naked eye somewhere near the turning point. Thus there is no sharp distinction between the branches A_1 and A_2 and no bifurcation is associated with the transformation of the streamlines of A_1 into those of A_2.

This transformation continues along A_2, which at its end looks like a pure $n=3$ state. Indeed, the resulting bifurcation can be detected as a $d=1/3$ instability of the $n=3$ state. Clearly, this type of gradual transition is only possible between states of like symmetry, and it is this property that makes the odd:odd resonances special. A similar statement applies to the bifurcation to B_2 and C from the $n=5$ state. It should be noticed that these bifurcations do *not* result in the

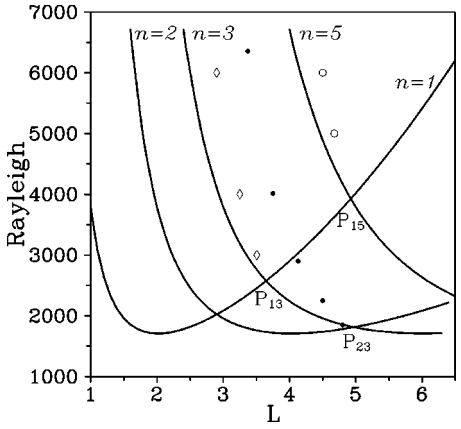

FIG. 6. The marginal stability curves for $n=1$, $n=2$, $n=3$, and $n=5$ modes (solid lines). Diamonds and open circles denote the points where $n=3$ and $n=5$ solutions bifurcate to families of hybrid solutions; full circles denote the points where the $n=3$ state acquires stability.

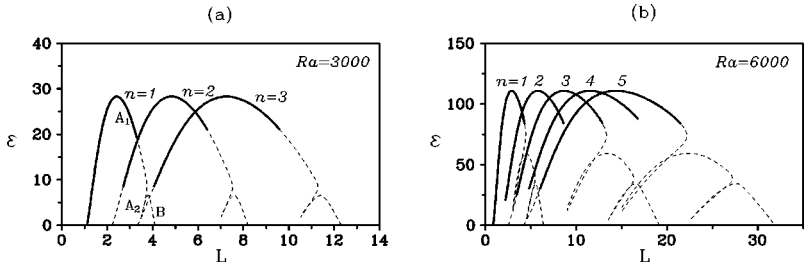

FIG. 7. Amplitude $\epsilon \equiv (1/2)v_x^2(L/4n,1/4)$ of different steady multiroll solutions for (a) Ra$=3000$ and (b) Ra$=6000$ as a function of the spatial period L for $\sigma=10$. Solid (broken) lines denote stable (unstable) solutions.

acquisition of stability by the $n=3$ and $n=5$ branches. As shown in Fig. 7 these branches, like $n=2$ and $n=4$, start out being unstable. This is because for both Ra$=3000$ and Ra $=6000$ the first instability is to the $n=1$ state. As shown below, the $n=3$ states acquire stability with increasing Ra only as a result of shedding a branch of R-symmetric states. The full circles in Fig. 6 indicate the location of this secondary bifurcation and suggest that this bifurcation is ultimately the consequence of the 2:3 resonance: the full circles all fall on a curve that appears to emerge from the point $P_{2,3}$ where this 2:3 resonance takes place. This resonance thus appears to be responsible for the stability of the $n=3$ multiroll solutions. Figure 7 summarizes the stability regions for the first few multiroll states as a function of the spatial period L for these two values of Ra.

It will have been noticed that there is a secondary bifurcation on the A_1 branch (see Figs. 2 and 3) at which this branch loses stability. As discussed below, this instability is associated with a bifurcation to a P-invariant state, and hence with the generation of a state that is accompanied by an antisymmetric mean flow. Bifurcations of this type are absent from the Eckhaus description valid close to threshold.

B. Transitions at constant spatial period

In this section we describe the corresponding results for $L=3$ and $L=3.8$ and increasing Rayleigh number; these values of L bracket the 1:3 resonance, which occurs at $(L^*,\mathrm{Ra}^*)\simeq(3.647,2574)$. The results are summarized in Fig. 8. These figures show all the nonlinear solutions we have computed together with their symmetries. The primary multiroll branches bifurcate from the conduction state in a sequence of bifurcations indicated in Fig. 1. For $L=3$, the successive primary bifurcations are to $n=2$, $n=1$, $n=3,\ldots$, while for $L=3.8$ the corresponding sequence is $n=2$, $n=3$, $n=1,\ldots$. The resulting Nusselt numbers are shown in Fig. 8 as a function of the Rayleigh number. All steady solutions obtained with $L=3$ and $L=3.8$ are included. Solid lines represent stable G-symmetric solutions; these solutions are stable with respect to *all* perturbations that fit in a domain of size $L(=na)$. The dashed lines indicate solutions of this type that are unstable, while the dotted indicate unstable solutions that are not invariant under the group G.

For $L=3$, the $n=1$ solutions that bifurcate from the conduction state at Ra$=2082$ belong to the family A_1 and are unstable at onset; they acquire stability at Ra$=2207$ and remain stable thereafter [Fig. 8(a)]. In contrast for $L=3.8$ the $n=1$ solution that appears in a primary bifurcation is of type B_1. This branch bifurcates from the conduction state at Ra $=2711$ and is unstable throughout. However, the other $n=1$ solutions are still present although they do not appear in a primary bifurcation. Instead the families A_1 and A_2 appear simultaneously at *finite* amplitude in a saddle-node bifurcation at Ra$=3175$ [Fig. 8(b)]. Initially both are unstable but the A_1 branch does acquire stability with increasing Rayleigh number. The streamlines of these three $n=1$ solutions A_1, A_2, B are displayed in Fig. 5 for Ra$=6000$. We surmise

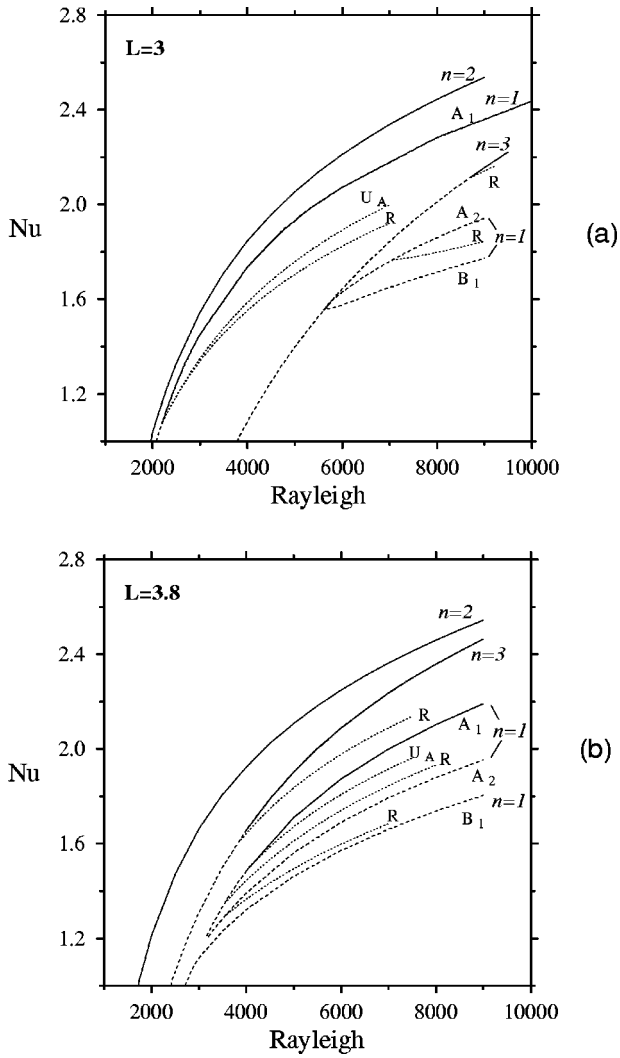

FIG. 8. Nusselt numbers of the steady solutions for (a) $L=3$ and (b) $L=3.8$ as a function of the Rayleigh number for $\sigma=10$. Solid (broken) lines indicate stable (unstable) G-symmetric solutions; dotted lines indicate unstable solutions with smaller symmetry.

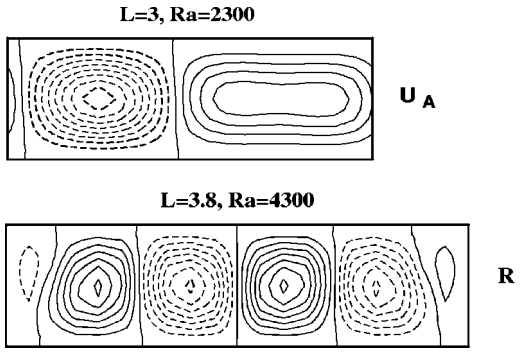

FIG. 9. Streamlines of (a) a steady P-symmetric solution with an antisymmetric mean flow profile U_A that bifurcates from an $n=1$ solution of type A_1 when $L=3$ and (b) a steady R-symmetric solution that bifurcates from an $n=3$ solution when $L=3.8$.

that the stable rolls computed in [14] are of type A_1 since the other $n=1$ states that coexist with this solution are all unstable. The A_1 solutions were found earlier by Prat *et al.* [5] in their study of mean flow generation in two-dimensional convection with spatial period $L=a$.

When $L=3$ and $L=3.8$ and the Rayleigh number is reduced the $n=1$ solutions belonging to family A_1 lose stability (see Figs. 2 and 3). This instability is caused by a perturbation with $d=0$, and gives rise to a P-symmetric state accompanied by a mean flow with an antisymmetric profile (denoted by U_A in Fig. 8). The instability of the $n=3$ multiroll solutions is caused by a $d=1/3$ perturbation that gives rise to a solution that breaks the basic period $L/3$ but preserves the reflection symmetry (denoted by R in Fig. 8). Both bifurcations are subcritical. For $L=3$, the $n=1$ solutions of type A_1 are unstable for $2082 \leqslant \mathrm{Ra} \leqslant 2207$, while the $n=3$ solutions are unstable for $3784 \leqslant \mathrm{Ra} \leqslant 8693$. In contrast, for $L=3.8$ the $n=1$ solutions of type A_1 are unstable for $3175 \leqslant \mathrm{Ra} \leqslant 4057$ while the $n=3$ solutions are unstable for $2412 \leqslant \mathrm{Ra} \leqslant 3825$ (see Fig. 8). The streamlines corresponding to the bifurcated solutions U_A and R are shown in Fig. 9: the U_A solution for $L=3$ is shown at $\mathrm{Ra}=2300$ while the R solution that bifurcates from the $n=3$ state when $L=3.8$ is shown at $\mathrm{Ra}=4300$.

Besides the bifurcations that stabilize the $n=1$ solutions of type A_1, we have also investigated the subsequent bifurcations as the Rayleigh number is reduced. Figure 8 shows that for both values of L considered a new steady R-symmetric solution bifurcates subcritically between the first appearance of the solution and the point where it gains stability. Figure 10 shows the streamlines of this solution when $L=3$ and $\mathrm{Ra}=2300$. In Table I we present the critical Rayleigh numbers for the secondary bifurcations giving rise to both types of solutions; for $L=3$ these occur at almost the same Rayleigh numbers, while for $L=3.8$ they are substantially farther apart. The former value is very close to the 1:2 resonance at $(L,\mathrm{Ra})=(2.92,2055)$ and this allows us to identify the U_A and R solutions with the *mean flow* and *transition* solutions identified in Refs. [6,7]. In contrast, when $L=3$ and Ra is reduced, the $n=3$ solutions undergo a transcritical bifurcation resulting in two branches of unstable solutions (A_2 and B_1) as already discussed [see Figs. 4(a) and 8(a)]. This bifurcation point falls on the line connecting the diamonds in Fig. 6.

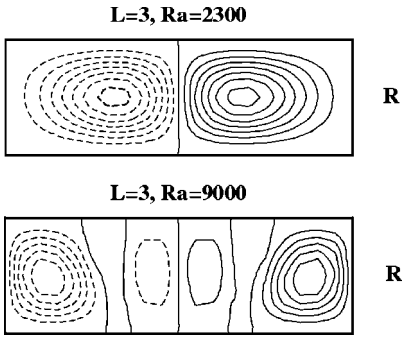

FIG. 10. Streamlines of two steady R-solutions, one bifurcating from an $n=1$ solution of type A_1 and the other bifurcating from an $n=1$ solution of type A_2, both for $L=3$.

We conclude the description of all the bifurcations that take place for the parameter values of Fig. 8 by considering another subcritical bifurcation that appears from the $n=1$ solutions of type A_2. This solution is G invariant and undergoes a $d=0$ instability that produces an R-invariant tertiary solution branch. These solutions are not accompanied by a mean flow. In Fig. 10 we show the streamlines for a solution of this type; here $L=3$ and $\mathrm{Ra}=9000$. A similar instability occurs when $L=3.8$ despite the different origin of the A_2 branch.

IV. THEORETICAL INTERPRETATION

A. The transcritical bifurcation

A number of the numerical results described above can be understood quite simply. The following discussion omits the complications arising from reflections in $z=0$ and consequently does not capture all the transitions identified in the preceding section. However, despite this shortcoming it does shed light on much of the observed behavior.

Consider first the secondary bifurcation from the $n=3$ state to the $n=1$ states described in Fig. 4(a). The $n=3$ state is invariant under translations by $L/3$; such translations may be viewed as rotations by $2\pi/3$. In addition this state is reflection invariant (cf. [15]). Consequently the $n=3$ state has the symmetry D_3 of rotations and reflections of an equilateral triangle. The observed steady state bifurcation from this state breaks this symmetry and can therefore be described in terms of an order parameter that measures the contribution from the symmetry breaking $n=1$ state. Equivariance with respect to the symmetry D_3 demands that this order parameter satisfy the equation

$$\dot{w} = -\lambda w + a\overline{w}^2 + b|w|^2 w + \cdots . \tag{4}$$

This equation is equivariant with respect to the operation $w \to we^{2i\pi/3}$; equivariance with respect to $w \to \overline{w}$ requires that

TABLE I. The critical Rayleigh number for secondary bifurcations from the $n=1$ branch A_1.

	U_A	R
$L=3$	2206.96	2206.90
$L=3.8$	4057	3545

the coefficients be real. These operations generate the group D_3 and represent rotation by 120° and reflection, respectively. The parameter λ is the bifurcation parameter and corresponds to the departure of the Rayleigh number from its critical value at the bifurcation. Its sign was chosen to agree with the numerical results: the pure $n=3$ state [corresponding to $w=0$ in Eq. (4)] has two unstable eigenvalues, each of double multiplicity to the left of the bifurcation and only one unstable eigenvalue (of double multiplicity) to the right. Consequently, it *gains* a pair of stable eigenvalues with increasing Rayleigh number, as described by the linearization of Eq. (4) about the $n=3$ state $w=0$.

Writing $w=\rho e^{i\theta}$ we obtain the two real equations

$$\dot{\rho}=-\lambda\rho+a\rho^2\cos 3\theta+b\rho^3, \quad \dot{\theta}=-a\rho\sin 3\theta.$$

The nontrivial fixed points are thus given by $\theta=\pi/3,2\pi/3$ modulo $2\pi/3$. We find two nontrivial solution branches emerging from the bifurcation, given by

$$\lambda=\mp a\rho+b\rho^2, \tag{5}$$

corresponding to $\theta=\pi/3,\theta=2\pi/3$, respectively. Each solution has two eigenvalues,

$$s=\mp a\rho+2b\rho^2, \quad s=\pm 3a\rho,$$

where ρ satisfies Eq. (5). Three observations follow immediately: there are two nontrivial branches that emerge from the bifurcation point, the bifurcation is transcritical, and the nontrivial solutions are unstable on either side of the bifurcation. In fact, regardless of the sign of a each branch has one stable and one unstable eigenvalue, and these eigenvalues are exchanged across the bifurcation. Moreover, one of the nontrivial solutions turns around with increasing amplitude. This occurs at a saddle-node bifurcation where a further change in stability takes place. If we choose the signs of a,b in accord with the numerical simulations, $a<0,b>0$, we find that it is the $\theta=2\pi/3$ branch that undergoes the saddle-node bifurcation: at small amplitude, as measured by Re w, the branch has eigenvalues $(-,+)$ while beyond the saddle-node bifurcation the eigenvalues are $(+,+)$. In contrast the branch $\theta=\pi/3$ increases monotonically with increasing λ and its stability remains $(+,-)$ throughout. The resulting bifurcation diagram is identical to Fig. 4(a) and the stability assignments are identical to those computed from the partial differential equations. In particular we have checked the change in the sign of the eigenvalues of the nontrivial solutions across the bifurcation at $\lambda=0$. Thus we can with confidence identify the $\theta=\pi/3$ branch with the A_2 state and the $\theta=2\pi/3$ state with the B_1 state. In fact the only difference between the above description and the numerics lies in the presence of an *additional* unstable eigenvalue of double multiplicity on the $n=3$ branch due to the prior loss of stability to the $n=2$ state [see Fig. 8(a)]. The midplane reflection symmetry also introduces complications. In fact we find that the $(+,-)$ eigenvalues of A_2 and the $(-,+)$ eigenvalues of B_1 lie in the G- and $T_{a/2}\kappa$-invariant subspaces, while each solution also has a positive eigenvalue in the R- and P-invariant subspaces. These additional unstable eigenvalues become equal along either branch as the bifurcation point $\lambda=0$ is approached. Thus numerically the state A_2 has three unstable eigenvalues while the state B_1 has three unstable eigenvalues between the bifurcation and the saddle-node but four unstable eigenvalues beyond it. The eigenvalue in the R-invariant subspace is responsible for the subsequent bifurcation from A_2 to the state labeled R in Fig. 8(a).

The secondary bifurcation from the $n=5$ state to the $n=1$ states seen in Fig. 3 can be analyzed in a similar way. The $n=5$ state is invariant under translations by $L/5$; such translations may be viewed as rotations by $2\pi/5$. Because of the reflection symmetry of the $n=5$ state this state has the symmetry D_5. The observed steady state bifurcation from this state breaks this symmetry and can therefore be described in terms of an order parameter that measures the contribution from the symmetry-breaking $n=1$ state. We obtain

$$\dot{w}=-\lambda w+a\bar{w}^4+b|w|^2w+\cdots, \tag{6}$$

where the coefficients a and b are again real. We choose the sign of the bifurcation parameter λ to agree with the numerical results: the pure $n=5$ state [corresponding to $w=0$ in Eq. (6)] has four unstable eigenvalues, each of double multiplicity, to the left of the bifurcation and three unstable eigenvalues (of double multiplicity) to the right. Consequently it *gains* a pair of stable eigenvalues with increasing Rayleigh number, as described by the linearization of Eq. (6) about the $n=5$ state $w=0$. In the partial differential equations this is a $d=1/5$ (equivalently $d=4/5$) instability.

As before, Eq. (6) can be written as two real equations

$$\dot{\rho}=-\lambda\rho+a\rho^4\cos 5\theta+b\rho^3, \quad \dot{\theta}=-a\rho^3\sin 5\theta.$$

The nontrivial fixed points are thus given by $\theta=\pi/5,2\pi/5$ modulo $2\pi/5$, and we find two *pairs* of nontrivial solution branches emerging from the bifurcation. These are given by

$$\lambda=\mp a\rho^3+b\rho^2,$$

and correspond to $\theta=\pi/5,4\pi/5$ and $\theta=2\pi/5,3\pi/5$, respectively. In a bifurcation diagram showing Re w as a function of λ each pair of solutions describes a pitchfork bifurcation, both of which bifurcate in the *same* direction. We choose $b>0$ and identify the larger amplitude branch (eigenvalues $+,-$) with the B_2 branch and the smaller amplitude branch (eigenvalues $+,+$) with the C branch. Figure 4(b) indicates that the coefficient a is in fact small. A more detailed investigation of the partial differential equations reveals that the instability takes place in the $T_{a/2}\kappa$-invariant subspace; in addition there are two distinct positive eigenvalues in each of the G-, R-, and P-invariant subspaces for both branches so that B_2 has 7 unstable eigenvalues, while C has 8 (see Sec. III).

B. The 1:3 spatial resonance

We now turn attention to Fig. 8(b) and in particular to the appearance of the disconnected branch of $n=1$ states and show that this type of behavior is a natural consequence of the 1:3 spatial resonance. As shown in Appendix B the 1:3 resonance is described by the amplitude equations

$$\dot{v}=(\mu+\delta)v+a|v|^2v+b|w|^2v+cw\bar{v}^2, \tag{7a}$$

$$\dot{w}=\mu w+d|v|^2w+e|w|^2w+fv^3, \tag{7b}$$

cf. [9,16]. Here v,w are the (complex) amplitudes of $n=1$ and $n=3$ modes, respectively, μ is the bifurcation parameter, and δ represents an unfolding parameter that splits apart the multiple bifurcation. These equations have rich dynamical behavior partially described in [9]. In the following we focus on the behavior that corresponds to that seen in the partial differential equations.

Equations (7) have the solution $(v,w)=(0,w)$ corresponding to a pure $n=3$ state. This state obeys the equation

$$\dot{w}=\mu w+e|w|^2w$$

and bifurcates supercritically at $\mu=0$ provided $e<0$. Its stability properties are specified by four eigenvalues one of which is zero because of translation invariance. The remaining three are $2e|w|^2$ and $\mu+\delta+b|w|^2$ (twice). The former is stable for a supercritical branch; the latter vanishes at a secondary steady state instability to a mixed state consisting of the $n=3$ mode with an admixture of an $n=1$ mode. We have seen above that such a bifurcation is *transcritical* [Fig. 8(a)].

In the following we shall emphasize the *hybrid* modes. These are steady state solutions of Eqs. (7) with $vw\neq 0$. We write $v=re^{i\theta},w=\rho e^{i\phi},\psi=\phi-3\theta$, obtaining

$$\dot{r}=(\mu+\delta)r+ar^3+b\rho^2r+cr^2\rho\cos\psi, \tag{8a}$$

$$\dot{\rho}=\mu\rho+dr^2\rho+e\rho^3+fr^3\cos\psi, \tag{8b}$$

$$\dot{\psi}=-\frac{r}{\rho}(fr^2+3c\rho^2)\sin\psi. \tag{8c}$$

It follows that there are two families of hybrid modes given by $\psi=0,\pi$. In the following we refer to these as $H_{0,\pi}$, respectively. Note that both are P symmetric.

These states obey

$$\mu+\delta+ar^2+b\rho^2\pm cr\rho=0, \tag{9a}$$

$$\mu\rho+dr^2\rho+e\rho^3\pm fr^3=0. \tag{9b}$$

As a result the amplitude ratio $\zeta\equiv\rho/r$ satisfies the single cubic equation

$$(\mu+\delta)f+[(\mu+\delta)d-\mu a]\zeta-\mu c\zeta^2+[(\mu+\delta)e-\mu b]\zeta^3=0.$$

Consequently, there are at most three solution branches at any given value of μ with $\zeta>0(<0)$ corresponding to $H_{0,\pi}$. The bifurcation from the conduction state (0,0) to the hybrid mode thus takes place at $\mu=-\delta$ $(\zeta=0)$ and is supercritical if $a<0$.

The stability of this branch is readily computed: both steady-state bifurcations corresponding to saddle-node bifurcations or the termination of the $n=1$ branch on the $n=3$ are present; Hopf bifurcations are also possible. Rather than providing a detailed discussion of these equations we demonstrate below that the equations do describe the transition from Fig. 8(a) to Fig. 8(b) as L is increased. Our choice of coefficients was guided by the coefficient values computed by MF for $\sigma=\infty$. These have been interpolated to obtain values corresponding to $L=3.647$: $a=-1.5205$, $b=-10.033$, $c=-0.82498$, $d=-9.0393$, $e=-11.8845$, $f=-0.2421$. Since our calculations are carried out substantially far from the mode interaction point corresponding to $\mu=\delta=0$ we do not expect these values to reproduce our results. In Fig. 11 we show the results obtained using $a=-4.5205$, $e=-5.8845$, and retaining the MF values for the remaining coefficients. The figures reveal bifurcation diagrams in excellent qualitative agreement with those of Fig. 8. In particular, for $\delta>0$ (i.e., $L<L_{1,3}$) we find the transcritical bifurcation from the $n=3$ state, while for $\delta<0$ $(L>L_{1,3})$ we recover the disconnected $n=1$ branch seen in Fig. 8(b).

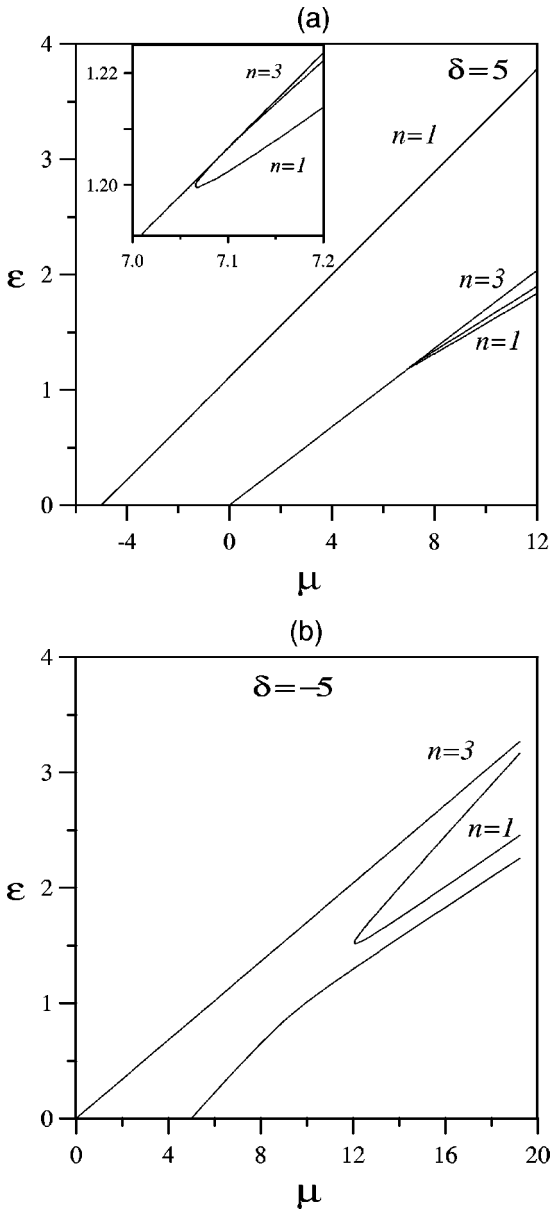

FIG. 11. Bifurcation diagrams $\varepsilon=\rho^2+r^2$ vs μ obtained from the amplitude Eq. (7) for (a) $\delta>0$, (b) $\delta<0$. (a) shows the transcritical bifurcation from the $n=3$ state (inset shows a detail) while (b) shows the disconnected $n=1$ branch. These figures should be compared with Figs. 8(a) and 8(b), respectively. For the coefficients see text.

The amplitude equations also allow us to determine the nature of the transition between these two diagrams. Setting $\delta = 0$ we find that Eqs. (7) reduce to four straight lines through $\mu = 0$. One of these is the $n = 3$ branch, which is always present. The other three lines all correspond to $n = 1$ states. We find that as $|\delta| \to 0$ the secondary bifurcations approach zero amplitude. As δ passes through zero and the order in which the primary bifurcations take place changes the secondary $n = 1$ branches present for $\delta > 0$ detach from the $n = 3$ branch producing a disconnected pair of $n = 1$ branches for $\delta < 0$. We conclude that the amplitude equations are capable of reproducing much of the structure revealed in the our numerical study, although they miss several important secondary instabilities that play an important role in the stabilization of the finite amplitude solution branches at moderate distance from the mode interaction point (cf. Fig. 8).

V. CONCLUSIONS

In this paper we have examined in detail both the existence and stability properties of different time-independent solutions of the partial differential equations describing two-dimensional Rayleigh-Bénard convection with periodic boundary conditions in the horizontal and identical no-slip boundary conditions at top and bottom. The paper identifies a number of complications that arise in the wave number selection process as a result of the presence of midplane reflection symmetry. These appear already at moderate Rayleigh numbers. To appreciate the significance of our results it is helpful to compare our Fig. 8 with an Eckhaus analysis in which this symmetry is absent, summarized in Fig. 2 of Ref. [10]. Although the two sets of figures have broad similarities they differ substantially in detail. In the Eckhaus picture the second mode to go unstable acquires the stability at a secondary pitchfork; in our problem two bifurcations are necessary, one to an R-symmetric state and the second to a P-symmetric state accompanied by a mean flow with an antisymmetric profile. The mode acquires stability only after the second of these, as found already in Refs. [6,7]. Such a state is absent from the Eckhaus description. In both figures the third unstable mode requires two bifurcations before acquiring stability. However, in the Eckhaus case both are simple pitchforks to reflection-symmetric states while in our Fig. 8(a) the first of these is transcritical and the reflection-symmetric state appears only in a tertiary bifurcation. It is tempting to surmise that our Fig. 8(a) would collapse into Fig. 2(b) of Ref. [10] if the midplane reflection symmetry characteristic of the present problem were absent. Similar statements can be made about our Fig. 8(b). Here the dominant new effect is the fact that the A_1 branch is disconnected from the trivial solution. We have seen that this is an effect of the 1:3 resonance and conclude that the $n = 1$ states studied by Bolton *et al.* [14] and Prat *et al.* [5] do not necessarily bifurcate from the conduction state: when the spatial period L exceeds that corresponding to the 1:3 resonance ($L^* = 3.647$) such solutions appear in turning point bifurcations as the Rayleigh number is increased. In this respect our calculations extend earlier work by Mizushima and Fujimura [9] on the 1:3 resonance and related work by Moore and Weiss on doubly diffusive convection [13]. The former employ amplitude equations valid near particular codimension-two points for their study of the Rayleigh-Bénard problem with no-slip boundary conditions. Although the range of validity of this approach is limited we find that the results remain qualitatively correct for Rayleigh numbers smaller than that for the next important resonance, the 1:5 resonance. The latter work is closer in spirit to that of the present paper, but differs from it in that the primary instability is typically subcritical. We have focused on the stability properties of secondary solutions arising from resonances of type $1{:}2k+1$ with $k = 1$ and $k = 2$. These resonances give rise to new $n = 1$ hybrid solutions involving both one and $2k+1$ pairs of rolls. These solutions branch with increasing spatial period L from the conduction state and have the same symmetries as a single pair of rolls. For spatial periods L smaller than that corresponding to a 1:3 resonance we found that the hybrid solutions terminate on the pure $n = 3$ $(k = 1)$ state via a transcritical bifurcation. In contrast in the 1:5 interaction both hybrid modes emerge from the $n = 5$ $(k = 2)$ state in the same direction. Additional interactions of the form $n-1{:}n, n > 2$, were also considered. These were found to be responsible for subcritical bifurcations from a pure n state and gave rise to a state with only reflection symmetry. Such a bifurcation also occurs in the Eckhaus analysis [10].

Throughout the paper we emphasized the important role played by the midplane reflection symmetry. We have seen that this symmetry is responsible for the importance of the 1:3 resonance. This is so despite the fact that the 1:2 resonance occurs at lower Rayleigh numbers and is a consequence of the fact that the leading order resonant term in the 1:2 interaction is of *higher* order than that in the 1:3 interaction. This in turn is a consequence of the fact that in the latter case the two interacting modes have similar symmetries and hence interact strongly; in contrast in the 1:2 resonance the two pure modes have different symmetries and the interaction between them must proceed via mixed modes, and this is so for any $k{:}k+1$ interaction in systems with Neumann or periodic boundary conditions [17]. At second order such modes generate modes with wave numbers 1 and $2k+1$ of which the former represents a large scale recirculating flow. Such flows are therefore associated with all mixed states of this type [18]. With stress-free boundary conditions at top and bottom these mixed modes may subsequently undergo a parity-breaking bifurcation to drifting states called traveling waves [7], although we have not found such solutions with no-slip boundary conditions. Note that for sufficiently small Prandtl numbers traveling (and modulated traveling) waves are present in the 1:3 resonance as well [9]. Such time-dependent states are absent for $\sigma = 10$. For this Prandtl number stable time-dependent states are present only at substantially larger Rayleigh numbers [5]. These states are typically chaotic but have a nonzero time-averaged mean flow reminiscent of that present in the experiments [1]. In contrast, the states with nonzero mean flow present at the moderate Rayleigh numbers studied here are all steady but unstable. However, despite this fact they play an important role in the wave number selection process.

ACKNOWLEDGMENTS

We wish to acknowledge the late Professor Josep Maria Massaguer for assistance and guidance. This work was sup-

ported by DGICYT under Grant No. PB94-1216 and by the National Science Foundation under Grant No. DMS-9703684.

APPENDIX A: CONVECTION ROLLS AND THEIR SYMMETRIES

In this appendix we briefly summarize some group-theoretic predictions about the symmetries of convection rolls and the types of secondary bifurcations that are allowed by these symmetries. These predictions can be made without an explicit representation of the roll state.

As pointed out in Sec. II the symmetry of the equations and boundary conditions is the group $O(2)\times Z_2$. The trivial (conduction) solution is invariant under this group. Consider first the primary bifurcation from this state. This bifurcation is a steady-state bifurcation and hence is described by a complex amplitude $A\in\mathbf{C}$, such that near onset [15]

$$\chi(x,z,t)=\mathrm{Re}\ A(t)e^{inx}f(z)+\cdots.$$

Here $f(z)$ is the vertical eigenfunction, assumed to be even in $z=0$. This solution describes the roll state, i.e., n pairs of rolls. By choosing the spatial period to be $2\pi/n$ instead of 2π we can set $n=1$ and focus on the symmetries of a single pair of rolls. This is the smallest possible period and represents one wavelength of the pattern. Since χ is a pseudoscalar under reflections the group $O(2)\times Z_2$ acts on $\mathbf{C}$ as follows:

$$\begin{aligned} \text{translations } T_l:&\quad A\to Ae^{il},\\ \text{reflections in } x=0\quad R_0:&\quad A\to-\overline{A},\\ \text{reflections in } z=0\quad \kappa:&\quad A\to -A. \end{aligned}\tag{A1}$$

By choosing the origin $x=0$ appropriately we can take A to be pure imaginary, say, $A=iA_0$. This solution is clearly invariant under R_0; thus the roll state is symmetric with respect to reflections in a vertical plane through a node. Moreover, both κ and T_π act by $-I$ and commute so that $T_\pi\kappa$ is a second symmetry. It is now easy to check that these are the only independent symmetries of iA_0. Since this solution is specified by a single real variable, viz., A_0, the equivariant branching lemma [19] guarantees the existence of a primary solution branch with the symmetry D_2, generated by R_0 and $T_\pi\kappa$. Note that T_π is a translation by half a wavelength, and that $U\equiv 0$ for this solution. The latter conclusion follows from the requirement that $U(z)=-U(z)$, which in turn follows from the symmetry R_0.

Consider now the operation $P=T_{\pi/2}R_0T_{-\pi/2}\kappa$. This is a reflection in $z=0$ followed by a reflection in $x=\pi/2$, instead of a reflection in $x=0$ (see Sec. II). One can easily check that iA_0 is invariant under P so that P is another symmetry of the primary roll state. Note that $P=T_{\pi/2}R_0T_{\pi/2}T_{-\pi}\kappa=R_0T_\pi\kappa$ so that P is not a *new* symmetry. As shown in Sec. II, P is also a symmetry of an *individual* roll; this symmetry is often called a *point* symmetry. As a consequence of ''hidden'' symmetry [20] the above considerations also apply to a roll solution computed with Neumann boundary conditions at $x=0$ and $x=\pi$.

The D_2 symmetry of the roll state can be broken in one of three ways. This is because the group D_2 has three nontrivial subgroups $\langle T_\pi\kappa\rangle$, $\langle R_0\rangle$, and $\langle R_0T_\pi\kappa\rangle$. All of these are simple reflections. As a consequence the perturbations of the roll state split into four classes, those that preserve the symmetry $G=D_2$ and those that preserve the shift-reflect, R and P symmetries, respectively, as discussed in Refs. [5,21]. This is so for both steady-state instabilities and Hopf bifurcations. Note that to reach these conclusions it is not necessary to write down explicit expressions either for the roll state or for the perturbations. In particular these conclusions apply to *fully* nonlinear roll states.

APPENDIX B: AMPLITUDE EQUATIONS FOR SPATIAL RESONANCES

In this appendix we summarize some well-known but nonetheless important properties of $1{:}n$ spatial resonances. In all cases we assume that $(\mathrm{Ra}-\mathrm{Ra}_{1,n})/\mathrm{Ra}_{1,n}\ll 1$, $(L-L_{1,n})/L_{1,n}\ll 1$ and write the stream function χ in the form

$$\chi(x,z,t)=\mathrm{Re}(ive^{ikx}+iwe^{inkx})f(z)+\cdots.$$

Here $f(z)$ is the vertical eigenfunction (assumed to be even in $z=0$) and v and w denote the complex amplitudes of the two modes. Since the system has $O(2)$ symmetry these amplitudes must satisfy equations equivariant with respect to the following two operations,

$$(v,w)\to(ve^{ikl},we^{inkl}),\quad (v,w)\to(\overline{v},\overline{w}),$$

corresponding, respectively, to translations $x\to x+l$ and reflections $x\to -x$. As in Appendix A we can set $k=1$ by choosing the basic period appropriately. The most general equations satisfying this requirement take the form

$$\dot{v}=pv+qw\overline{v}^{n-1},\quad \dot{w}=rw+sv^n,$$

where $p,\ldots,s$ are *real* invariant functions, i.e., functions of the three elementary invariants $|v|^2$, $|w|^2$, and $\mathrm{Re}\ \overline{v}^n w$. To third order in the amplitudes we therefore have [16]

$$\dot{v}=(\mu+\delta)v+a|v|^2v+b|w|^2v+cw\overline{v}^{n-1},$$

$$\dot{w}=\mu w+d|v|^2w+e|w|^2w+fv^n.$$

Here μ is the bifurcation parameter and δ represents an unfolding parameter that splits apart the multiple bifurcation. In the following we focus in the cases $n=2$ (1:2 resonance) and $n=3$ (1:3 resonance). In both cases there is a pure n solution of the form $(v,w)=(0,w)$ but no corresponding solution $(v,w)=(v,0)$. The dynamics of the $n=2$ equations are analyzed in detail in [8] while the $n=3$ case is studied in [9].

In the present problem the symmetry group Γ is $O(2)\times Z_2$ and not $O(2)$. The midplane reflection $\kappa\in\mathrm{Z}_2$ takes (v,w) into $(-v,-w)$ whenever $f(z)$ is even; otherwise it has no effect. This is because the stream function χ is a pseudoscalar under reflections. Since $f(z)$ is even for the modes of interest here the extra reflection cannot be omitted. This requires a change in the amplitude equations describing the 1:2 resonance, which now read [7]

$$\dot{v} = (\mu + \delta)v + a|v|^2 v + b|w|^2 v + c w^2 \overline{v}^3,$$

$$\dot{w} = \mu w + d|v|^2 w + e|w|^2 w + f v^4 \overline{w}.$$

In these equations we have retained only the lowest order resonant terms; three other nonresonant fifth order terms in each equation have been omitted. Observe that the midplane reflection symmetry has had a dramatic effect on the structure of these equations. Pure $n=1$ solutions $(v,0)$ now exist. Moreover, pairs of *mixed* modes of the form (v,w), $vw \neq 0$, and symmetries P and R bifurcate simultaneously from the pure modes, and are responsible for the stabilization of both pure modes at larger amplitudes [7]. As shown by Dangelmayr [16] these properties are common to all so-called weak spatial resonances. Thus the presence of the midplane reflection symmetry is responsible for changing a strong spatial resonance into a weak one.

The situation is quite different when $n=3$. The corresponding equations already commute with the midplane reflection and thus require no modification. The lowest order resonant terms are cubic. The resulting equations have a pure $n=3$ solution $(0,w)$ but no solution of the form $(v,0)$. Instead there is a hybrid solution (v,w), $vw \neq 0$, that bifurcates from the trivial state. This solution has the same symmetry as the $n=3$ solution and hence interacts with it strongly in the nonlinear regime; no intermediate branches of mixed parity are necessary. For this reason the 1:3 resonance is the dominant resonance for problems with midplane reflection symmetry.

The derivation of the mode interaction equations given above is valid only in the neighborhood of an appropriate codimension-two point $(\mathrm{Ra}_{1,n}, L_{1,n})$, namely, the intersection points of the neutral stability curves shown in Fig. 1. In this derivation the two unfolding parameters (called μ and δ in Sec. IV C) enter in the linear terms only. Under appropriate nondegeneracy conditions the nonlinear coefficients can be calculated *at* the multiple bifurcation point (i.e., at $\mu=\delta=0$) and hence are *independent* of both the Rayleigh number and the spatial period. The resulting equations are formally valid when $(\mathrm{Ra}-\mathrm{Ra}_{1,n})/\mathrm{Ra}_{1,n} \ll 1$, $(L-L_{1,n})/L_{1,n} \ll 1$. If these conditions are not satisfied the amplitude equations cannot be truncated and the results may be affected by other modes not included. For this reason the full partial differential equations must be used to explore the effects of spatial resonances away from the codimension-two points, as in the present paper.

[1] R. Krishnamurti and L. N. Howard, Proc. Natl. Acad. Sci. USA **78**, 1981 (1981); L. N. Howard and R. Krishnamurti, J. Fluid Mech. **170**, 385 (1986).

[2] J. W. Deardorff and G. E. Willis, J. Fluid Mech. **23**, 337 (1965); J. M. Finn, J. F. Drake, and P. N. Guzdar, Phys. Fluids B **4**, 2758 (1993); J. M. Finn, *ibid.* **5**, 415 (1993).

[3] P. C. Matthews, M. R. E. Proctor, A. M. Rucklidge, and N. O. Weiss, Phys. Lett. A **183**, 69 (1993); A. M. Rucklidge and P. C. Matthews, in *Theory of Solar and Planetary Dynamos*, edited by M. R. E. Proctor, P. C. Matthews, and A. M. Rucklidge (Cambridge University Press, Cambridge, 1993), p. 257.

[4] M. R. E. Proctor, N. O. Weiss, D. P. Brownjohn, and N. E. Hurlburt, J. Fluid Mech. **280**, 227 (1994).

[5] J. Prat, J. M. Massaguer, and I. Mercader, Phys. Fluids **7**, 121 (1995).

[6] F. H. Busse and A. C. Or, ZAMP **37**, 608 (1986).

[7] D. Armbruster, Physica D **27**, 433 (1987).

[8] C. A. Jones and M. R. E. Proctor, Phys. Lett. A **121**, 224 (1987); M. R. E. Proctor and C. A. Jones, J. Fluid Mech. **188**, 301 (1988); D. Armbruster, J. Guckenheimer, and P. Holmes, Physica D **29**, 257 (1988).

[9] J. Mizushima and K. Fujimura, J. Fluid Mech. **234**, 651 (1992).

[10] L. S. Tuckerman and D. Barkley, Physica D **46**, 57 (1990).

[11] I. Mercader, M. Net, and A. Falques, Comput. Methods Appl. Mech. Eng. **91**, 1245 (1991).

[12] J. Prat, Ph.D. Thesis, Universitat Politècnica de Catalunya (1996).

[13] D. R. Moore and N. O. Weiss, in *The Dynamics of Numerics and the Numerics of Dynamics*, edited by D. S. Broomhead and A. Iserles (Clarendon Press, Oxford, 1992), p. 107.

[14] E. W. Bolton, F. H. Busse, and R. M. Clever, J. Fluid Mech. **164**, 469 (1986).

[15] J. D. Crawford and E. Knobloch, Annu. Rev. Fluid Mech. **23**, 341 (1991).

[16] G. Dangelmayr, Dyn. Stab. Systems **1**, 159 (1986).

[17] H. Kidachi, Prog. Theor. Phys. **68**, 49 (1982); E. Knobloch and J. Guckenheimer, Phys. Rev. A **27**, 408 (1983); P. Metzener, Phys. Fluids **29**, 1373 (1986).

[18] In finite domains with non-Neumann boundary conditions at the lateral walls large scale flows are generated by a different mechanism. See P. Hirschberg and E. Knobloch, J. Nonlinear Sci. **7**, 537 (1997).

[19] M. Golubitsky, I. Stewart, and D. G. Schaeffer, *Singularities and Groups in Bifurcation Theory*, Vol. II (Springer-Verlag, New York, 1988).

[20] J. D. Crawford, M. Golubitsky, M. G. M. Gomes, E. Knobloch, and I. N. Stewart, in *Singularity Theory and its Applications, Warwick 1989, Part II*, edited by M. Roberts and I. Stewart, Lecture Notes in Mathematics Vol. 1463 (Springer, Berlin, 1991), p. 63.

[21] N. O. Weiss, in *Nonlinear Evolution of Spatio-Temporal Structures in Dissipative Continuous Systems*, edited by F. H. Busse and L. Kramer (Plenum Press, New York, 1990), p. 359; D. R. Moore, N. O. Weiss, and J. M. Wilkins, J. Fluid Mech. **233**, 561 (1991); M. R. E. Proctor and N. O. Weiss, Geophys. Astrophys. Fluid Dyn. **70**, 137 (1993).